Thermal acoustic excitations with atomic-scale wavelengths in amorphous silicon

Jaeyun Moon
Division of Engineering and Applied Science, California Institute of Technology, Pasadena, California 91125, USA

Raphaël P. Hermann and Michael E. Manley
Material Science and Technology Division, Oak Ridge National Laboratory, Oak Ridge, Tennessee 37831, USA

Ahmet Alatas and Ayman H. Said
Advanced Photon Source, Argonne National Laboratory, Argonne, Illinois 64039, USA

Austin J. Minnich*
Division of Engineering and Applied Science, California Institute of Technology, Pasadena, California 91125, USA

(Received 4 February 2019; revised manuscript received 6 May 2019; published 3 June 2019)

The vibrational properties of glasses remain a topic of intense interest due to several unresolved puzzles, including the origin of the Boson peak and the mechanisms of thermal transport. Inelastic scattering measurements have revealed that amorphous solids support collective acoustic excitations with low THz frequencies despite the atomic disorder, but these frequencies are well below most of the thermal vibrational spectrum. Here, we report the observation of acoustic excitations with frequencies up to 10 THz in amorphous silicon. The excitations have atomic-scale wavelengths as short as 6 Å and exist well into the thermal vibrational frequencies. Simulations indicate that these high-frequency waves are supported due to the high group velocity and monatomic composition of a-Si, suggesting that other glasses with these characteristics may also exhibit such excitations. Our findings demonstrate that a substantial portion of thermal vibrational modes in amorphous materials can still be described as a phonon gas despite the lack of atomic order.

DOI: 10.1103/PhysRevMaterials.3.065601

I. INTRODUCTION

Amorphous materials possess a number of peculiar vibrational properties compared to those of their crystalline counterparts [1–7]. For vibrations of frequency less than a few THz, the wavelengths are sufficiently long that the vibrational properties would be expected to be unaffected by the atomic disorder [8]. However, the observed density of states and heat capacity of glass differ from the Debye predictions at low temperatures below 10 K [1–7]. Various explanations have been proposed for these observations, including the soft potential model [9,10], elastic heterogeneities [11], and lower mass density of amorphous solids compared to their crystalline counterparts [6,7].

The introduction of high-brilliance inelastic x-ray scattering (IXS) experiments has enabled acoustic excitations to be resolved by wave vector and energy outside of the dynamic range accessible by neutron scattering [12–16]. The measurements have shown that many glasses [17–22] and liquids [23–26] support isotropic acoustic excitations with frequencies up to ∼1 THz despite the atomic disorder. Further, the observed inelastic peaks exhibit a broadening, $\Gamma(q)$, that increases with wave vector q following a power law [17–22,25–30]. The acoustic excitation ceases to be well-defined when the broadening is on the order of the frequency of the excitation, typically around a few THz. These general trends have been reported in a variety of glasses including polymers [18,28,30], metallic glasses [21], and monatomic glasses such as selenium [20], and others [17,19,22,27,29].

Numerical methods such as molecular dynamics simulations are often utilized to gain microscopic understanding of vibrational properties in amorphous materials and to guide experimental measurements. Amorphous silicon has been used for decades as a representative material to understand the vibrational properties of amorphous materials due to its monoatomic composition and widely used available potentials such as Stillinger-Weber [31,32] and Tersoff [33,34]. Prior computational works based on normal mode decomposition have concluded that propagating acoustic waves exist up to ∼2 THz to 3 THz [35–40] and that nonpropagating vibrations dominate the thermal conductivity [35,37–40]. On the other hand, recent calculations predicted that acousticlike vibrations are present well into the thermal frequencies [41,42]. The conflict between these reports remains unresolved due to the lack of inelastic scattering measurements that provide direct information on the acoustic excitations supported in a-Si.

Here, we report the observation of acoustic excitations with atomic-scale wavelengths as small as 6 Å, corresponding to frequencies up to 10 THz using IXS. Molecular dynamics simulations show that these high-frequency acoustic waves are supported due to the high group velocity and monatomic composition of a-Si, and that these results hold for a

*aminnich@caltech.edu

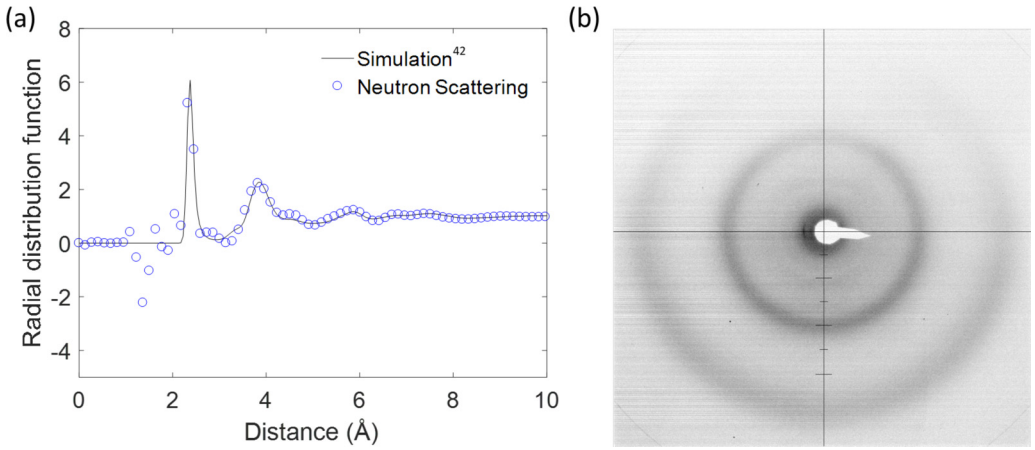

FIG. 1. Structural characterization of a-Si powders. (a) Radial distribution function (blue circles) of the sample A1 compared to a calculation using an amorphous structure from molecular dynamics (line) [42]. (b) X-ray diffraction pattern measured at 300 K. Each tick mark represents $2\theta = 2.5^\circ$ at x-ray energy of 21.657 keV. Broadened features in both the RDF and XRD measurements indicate an amorphous atomic structure.

variety of atomic configurations that match the observed radial distribution function (RDF). Such excitations extending in the thermal frequencies might also be found in other elastically stiff monatomic glasses such as tetrahedral amorphous carbon. Our findings indicate that the phonon gas model describes thermal atomic vibrations accurately in amorphous Si despite the lack of atomic order.

II. SAMPLE PREPARATION

We prepared two samples (A1 and A2) by depositing amorphous Si onto sapphire substrates by plasma-enhanced chemical vapor deposition (PECVD) at separate times with silane gas diluted (5%) in argon gas at a deposition table temperature of 473 K. To make the samples suitable for the x-ray beam with absorption length of 2 mm, the thin films (3 μm thick) were powderized in a glovebox under either nitrogen or argon and placed in quartz capillary tubes with 10 μm wall thickness. The structural characterization of sample A1 is shown in Fig. 1. The RDF of this sample was measured by neutron scattering at Nanoscale-Ordered Materials Diffractometer (NOMAD), Spallation Neutron Source (SNS) at Oak Ridge National Laboratory. The neutron total scattering structure function was produced by normalizing the sample scattering intensity to the scattering intensity from a solid vanadium rod and subtracting the background of an empty 2-mm quartz capillary. The radial distribution function was obtained through the Fourier transform of the total scattering function with momentum transfer between 0.1 and 31.4 Å^{-1}. The RDF and x-ray diffraction pattern show broadened features, indicating that the samples are disordered. The RDF indicates that residual hydrogen (~20 at. %) is present in the sample as indicated by the negative peak at the Si-H 1.4 Å distance, but we expect little influence on our measurements, considering that prior work observed no systematic change in thermal conductivity of PECVD amorphous silicon films with hydrogen content varying from 1 at. % to 20 at. % [43].

III. RESULTS

A. Inelastic x-ray scattering measurements

Dynamic structure factors from both samples (A1 and A2) were independently measured using spectrometers at sector HERIX-3 and HERIX-30 with energies of 21.657 and 23.71 keV at the Advanced Photon Source [44–47], respectively. The measurements for the longitudinal branch at different momentum transfers at room temperature are shown in Figs. 2(a) and 2(b), respectively. For both samples, distinct inelastic peaks are clearly visible at thermal frequencies up to around 10 THz, indicating the presence of collective acoustic excitations with well-defined frequencies and wave vectors. The wavelengths of these excitations are as small as 6 Å, comparable to the interatomic spacing in a-Si. A sudden increase in the broadening of the inelastic peaks is observed between 7.79 nm^{-1} and 11.12 nm^{-1} for A1 and between 10.0 nm^{-1} and 12.0 nm^{-1} for A2, respectively. This visual observation indicates that collective excitations with well-defined wave vectors and frequencies are not supported beyond these wave vectors and frequencies.

To determine the center frequencies and the broadening of the collective excitations at each momentum transfer, the dynamic structure factor spectra were modeled with a function $S(q, \nu)$ consisting of a Lorentzian for the central elastic peak and a damped harmonic oscillator for the inelastic peaks,

$$S(q,\nu) = I_0(q)\frac{\Gamma_0(q)^2}{\Gamma_0(q)^2+\nu^2} + [n(\nu)+1]I(q) \times \frac{\nu\Gamma(q)^2\Omega(q)}{[\Omega(q)^2-\nu^2]^2+\Gamma(q)^2\nu^2}, \quad (1)$$

where q is the wave vector, ν is the frequency, $I_0(q)$ and $\Gamma_0(q)$ are the intensity and width of the central peak, $I(q)$ and $\Gamma(q)$ are the intensity and full width half maximum of the inelastic peak with the peak frequency $\Omega(q)$, and $n(\nu)$ is the Bose factor [23]. The function $S(q, \nu)$ is then convolved with a pseudo-Voigt function representing the resolution function to fit to the experimental data [44].

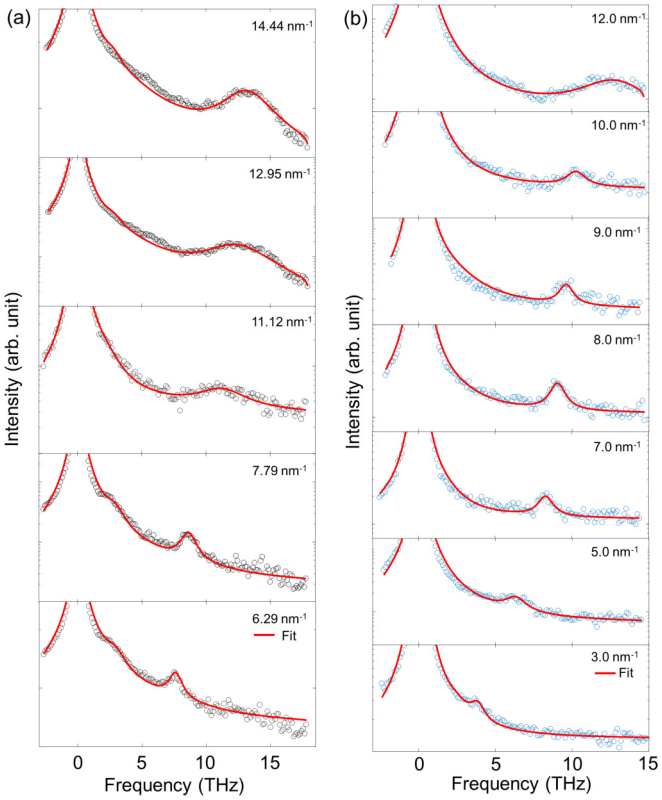

FIG. 2. Inelastic x-ray scattering spectra of (a) sample A1 (black circles) and (b) sample A2 (blue circles) along with the fit (red lines). For both samples, sharp inelastic peaks are observed at frequencies approaching 10 THz, above which a significant increase in the broadening is seen.

The dispersion relations of the measured acoustic excitations are plotted in Fig. 3 along with the calculated dynamic structure factor from Ref. [42]. The vertical bars represent the full width at half maximum of the inelastic peaks. Excellent agreement between the simulation and the IXS measurements is observed, with the sound velocities agreeing to within 4%. We attempted to include the 20 at. % hydrogen present in the sample in MD simulations using available interatomic potentials [48]; however, the thermal conductivity of the structure was inconsistent with experiments [49]. This discrepancy may arise because the interatomic potential was optimized for structural rather than dynamic properties. The good agreement between simulations with pure a-Si and experiments suggests that the presence of hydrogen does not affect the dispersion of the acoustic excitations. In both simulations and experiments, vibrations with frequencies less than ∼10 THz have a well-defined frequency and wave vector. As shown in Fig. S1 in the Supplemental Material [50], the calculated dynamic structure factors of Refs. [38,41] are also in good agreement with the measurements. These works also utilized Stillinger-Weber potential [31]. Comparison with other theoretical studies that focus on quantities of relevance to Allen-Feldman theory [35,51] is difficult because such quantities are not directly measured in an IXS experiment.

Next, we performed additional temperature-dependent IXS measurements on Sample A1 at 35 K and 500 K. The extracted inelastic peak frequencies and broadenings are shown in Fig. 4. We observe a slight softening with temperature for the peak frequency, $\Omega(q)$, but no temperature dependence of the broadening is seen. This observation indicates that the origin of the broadening of the inelastic peaks is structural rather than anharmonic. The temperature independence of the broadening has also been reported in other amorphous solids such as glycerol and silica [19,27,52].

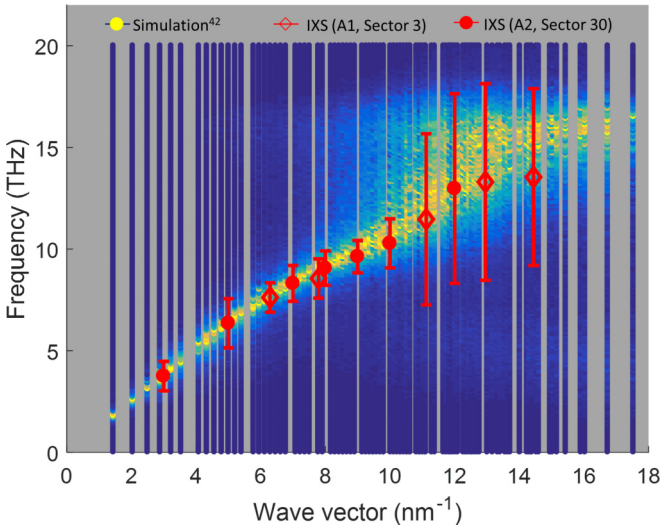

FIG. 3. Dispersion relation from IXS measurements (diamonds from sample A1 using HERIX sector 3 and filled circles from sample A2 using HERIX sector 30) and calculated dynamic structure factor from Moon *et al.* [42]. Vertical bars represent the FWHM of the inelastic peaks. The sound velocity from the measurements is 7850 m s^{-1}, within 4% of the predicted sound velocity of 8179 m s^{-1}.

IV. DISCUSSION

A. Dynamic structure factor of various atomic configurations

We note that a-Si does not have a uniquely determined structure. Prior calculations [53,54] have shown that paracrystalline amorphous silicon structures yield an RDF that is indistinguishable with that of experiments. We therefore generated three different amorphous silicon configurations (continuous random network, melt-quench, and crystal seed nucleation) that closely match with our RDF from neutron scattering. All three structures contain 4096 atoms and use the same SW potential with a time constant of 0.5 fs. The continuous random network model was provided by N. Mousseau and was generated from the modified Wooten-Winer-Weaire algorithm [55]. The description of the melt-quench method is provided in detail in Moon *et al.* [42]. For the crystal seed nucleation method, the crystalline silicon was first melted at 3500 K at constant volume for 50 ps while the spherical crystal seed atoms (1 at. %) are kept fixed at their positions. We then quenched the structure to 1000 K at 100 K ps^{-1}. The entire structure was then annealed at 1000 K and 0 bar for 2.75 ns in NPT followed by quenching to room temperature at the same rate as before. The resulting structure from the crystal seed nucleation, therefore, has a crystalline region as shown in Fig. 5(a). Only the crystallite atoms are displayed in the otherwise amorphous domain.

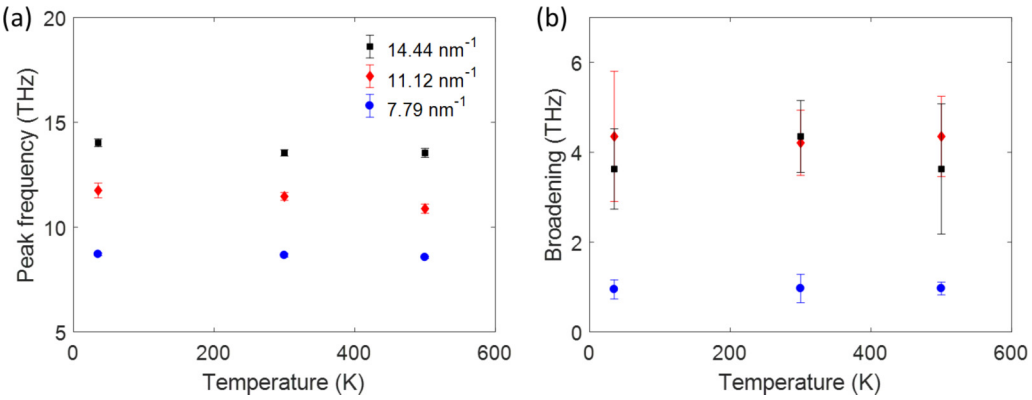

FIG. 4. Temperature-dependent IXS measurements for sample A1. (a) Inelastic peak frequency and (b) broadening at wave vectors of 7.79 (blue circles), 11.12 (red diamonds), and 14.44 nm^{-1} (black squares) at various temperatures. A slight softening of the peak frequencies with temperature is observed but no clear temperature dependence is found for the broadenings.

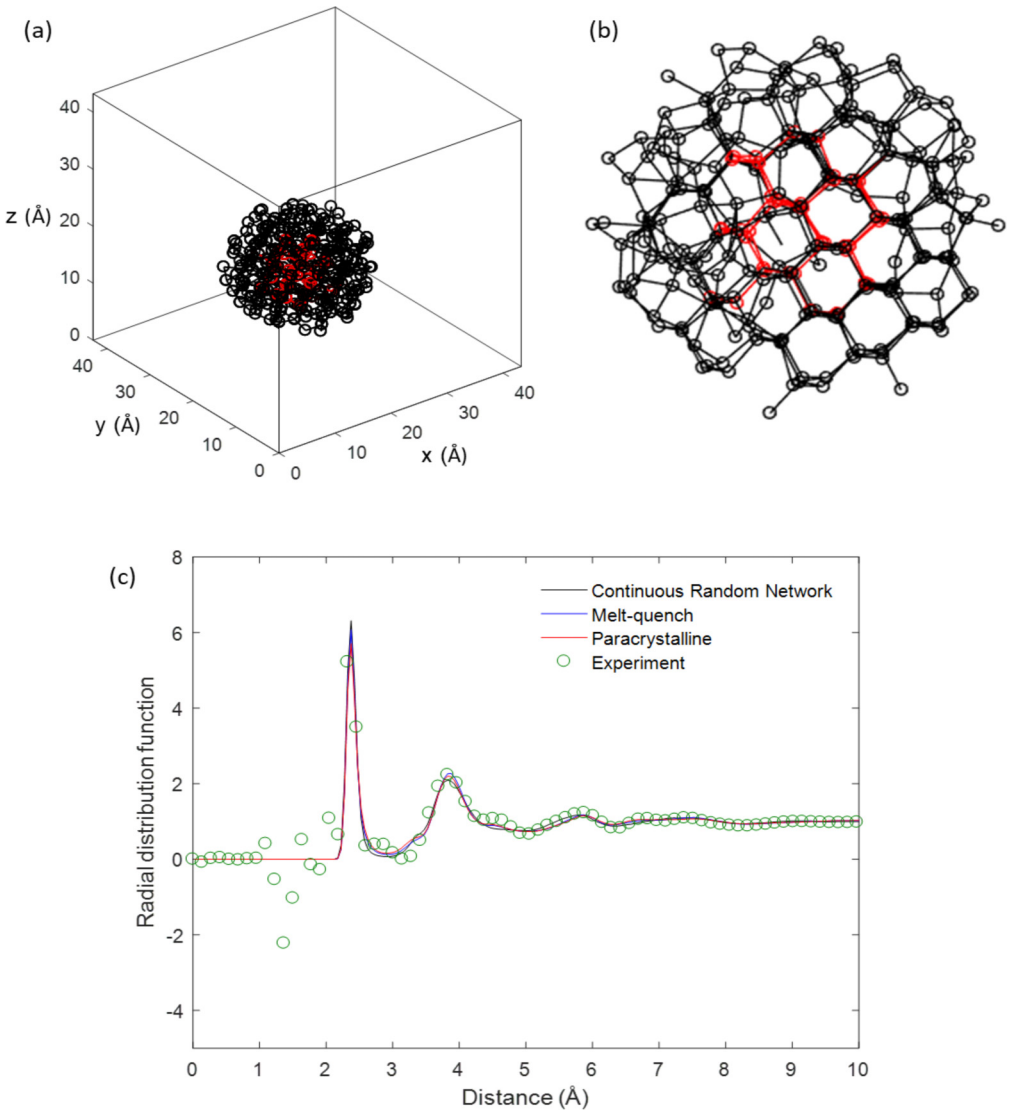

FIG. 5. (a) Paracrystalline amorphous silicon structure with only the crystalline region displayed. (b) Zoomed-in view of the crystallite. The red atoms denote the initial crystal seed and the black atoms represent the crystal growth from annealing. The crystallite is estimated to compose 8 at. % of the structure. Crystalline order is clearly observed. For scale, the average interatomic distance is around 2.35 Å. (c) Radial distribution function of continuous random network (black line), melt-quench (blue line), and paracrystalline (red line) amorphous silicon structures compared to that of experimental data (green circles).

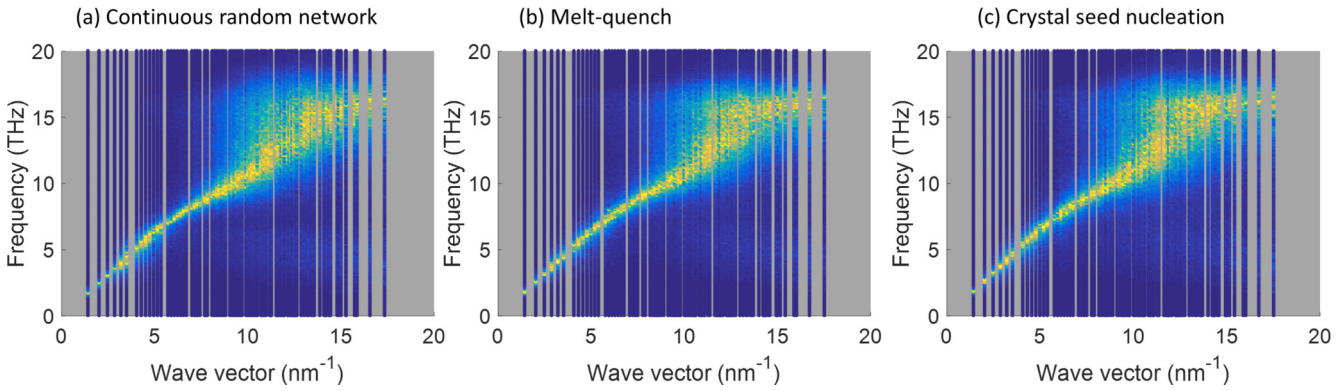

FIG. 6. Dispersion relations for longitudinal waves for (a) continuous random network, (b) melt-quench, and (c) crystal seed nucleation amorphous silicon structures. All of them show a crisp phonon dispersion up to around 10 THz, above which a significant broadening is observed.

A zoomed-in view of the crystallite is depicted in Fig. 5(b). The red atoms denote the initial crystal seed (1 at. %) and the black atoms represent the crystal growth from the seed during the annealing process. The crystalline region with well-defined tetrahedral local structures is easily observed and is estimated to be 8 at. % by dividing the number of atoms in the crystallite by the total number of atoms. The RDFs of the above-mentioned structures are plotted against the experimental data from neutron scattering in Fig. 5(c) and show good agreement. A larger crystal seed with 3 at. % was also used to create a paracrystalline silicon structure with the same procedure above, but additional distinctive peaks were clearly seen in the RDF, suggesting that the structural heterogeneity is large enough to affect the sample average of atomic density fluctuations.

The calculated dynamic structure factors of these three amorphous silicon structures are depicted in Fig. 6. We observe that all structures exhibit crisp phonon dispersion lines up to around 10 THz above which significant broadening is clearly observed, consistent with our IXS measurements. Comparisons of the RDFs and dynamic structure factor calculations between the PECVD a-Si and three amorphous silicon models suggest that acoustic excitations with frequencies up to 10 THz with atomic scale wavelengths exist in several possible atomic configurations of a-Si.

B. IXS measurement comparison among several amorphous materials

The broadening of the inelastic peaks, $\Gamma(q)$, of a-Si at 300 K versus wave vector are shown in Fig. 7(a) along with those of various types of amorphous materials from metallic glasses to polymers studied by IXS [18,21,27,30] and the computational work of Ref. [42]. A $\Gamma(q)$ α q^2 scaling is also shown as a guide to the eye. Previous works in other materials show a clear power-law dependence. In contrast, the

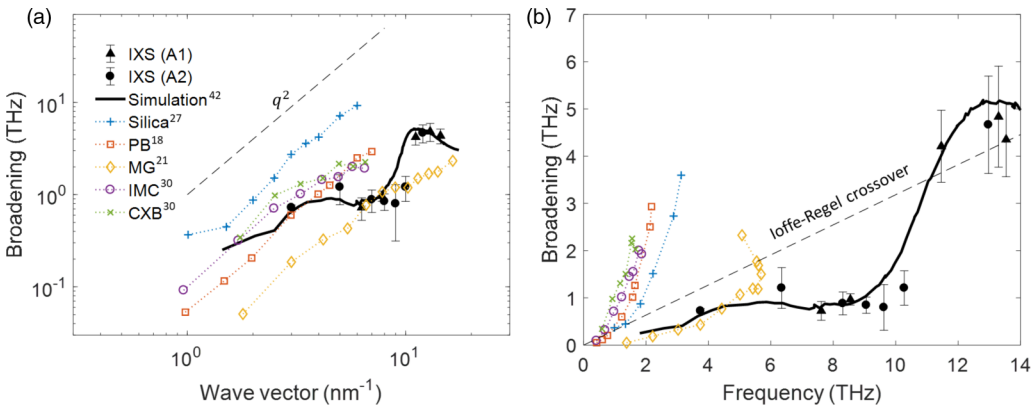

FIG. 7. Inelastic peak broadening for a-Si (A1 and A2) and other amorphous materials. (a) Broadening Γ versus wave vector q of various amorphous materials from IXS: Present measurements at 300 K (black filled triangles for A1 and black filled circles for A2), simulations from Ref. [42] (solid black line), silica at 1050 K (blue crosses) [27], polybutadiene at 140 K (PB, orange squares) [18], $Ni_{33}Zr_{67}$ metallic glass at room temperature (MG, yellow diamonds) [21], and amorphous drugs of Indomethacin (IMC, purple circles) and Celecoxib (CXB, green crosses) at room temperature [30]. A temperature dependence of the broadenings were not observed in these materials; therefore, direct comparison of our measurements at 300 K is possible. The q^2 dependence of broadening on wave vectors for these materials is not observed in amorphous silicon. (b) Broadening versus frequency for the same materials as in (a). The dotted line is the Ioffe-Regel crossover defined by $\Omega = \pi\Gamma$. The Ioffe-Regel crossover occurs at around $\sim$10 THz for a-Si, well into the thermal frequencies. The vertical bars in the measured data are the uncertainties of fitting the damped harmonic oscillator model to the measurements. The simulated broadening lies within the vertical bars.

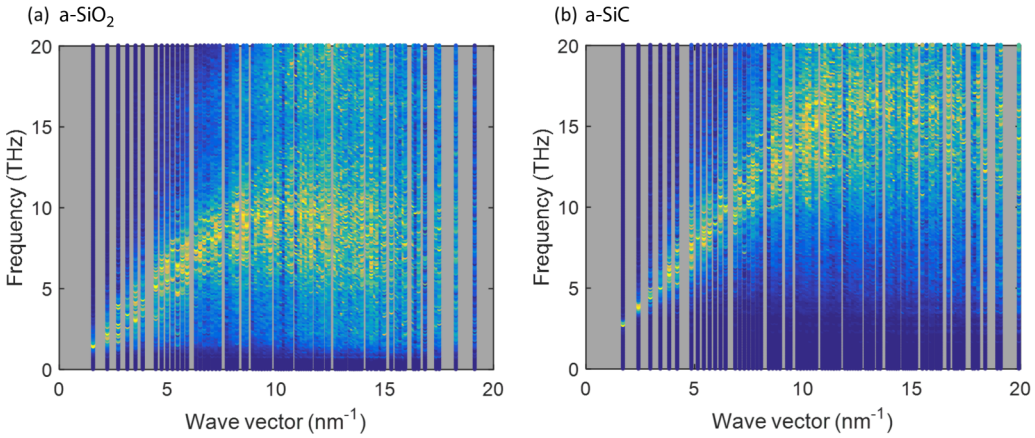

FIG. 8. Calculated dynamic structure factor for longitudinal vibrations in (a) a-SiO_2 and (b) a-SiC. Noticeable broadening is observed for frequencies below 10 THz. The Ioffe-Regel crossover frequency is ∼1.5 THz and ∼8 THz for (a) and (b), respectively.

broadening of a-Si for both the IXS and dynamic structure factor calculations [41,42] demonstrate a sudden increase rather than a power-law dependence. This sudden increase with frequency in the broadening can also be visually observed in the raw data shown in Fig. 2. The origin of this increase is at present not clear and will be the subject of future work.

The definition of the frequency at which an acoustic excitation is no longer well-defined is conventionally taken to be when the broadening $\Gamma(q) = \Omega(q)/\pi$, known as the Ioffe-Regel crossover [2,56]. Using this criterion, we find a strikingly high crossover frequency of around 10 THz, as shown in Fig. 7(b). This crossover frequency (corresponding to $\hbar\omega/k_B = 480\,\mathrm{K}$) is well within the portion of the vibrational spectrum thermally occupied at 295 K and implies that acoustic excitations are supported for wavelengths as small as ∼6 Å, only a few times larger than the interatomic distance of amorphous silicon (∼2.4 Å).

Our simulations show that this unusually high crossover frequency can be explained by two features of a-Si. First, acoustic excitations cease to possess a well-defined wave vector and frequency if the disorder is sufficiently strong. a-Si is monatomic with only minor isotopic mass disorder and hence lacks the degree of disorder present in polyatomic glasses such as mass or force constant disorder. Using Tersoff potentials [34,57], dynamic structure factors of a-SiO_2 and a-SiC were calculated. The longitudinal sound velocities of a-SiO_2 and a-SiC from dynamic structure factors are calculated to be 5567 and 9844 $\mathrm{m\,s^{-1}}$, which are within 5% of the experimental results of 5800 and 9462 $\mathrm{m\,s^{-1}}$, respectively [27,58]. Clear additional broadening in the dispersions is observed compared to a-Si as shown in Fig. 8.

Second, a-Si has a high group velocity due to the low atomic mass of Si and stiff covalent bonds. Thus, for a given wave vector, a-Si supports higher frequency excitations than for a heavier and weaker bonded amorphous material like glassy selenium. Inelastic neutron and x-ray scattering studies on glassy selenium reported a longitudinal sound velocity of around 2000 $\mathrm{m\,s^{-1}}$, leading to a Ioffe-Regel crossover frequency of around 1–2 THz [20,59]. For a given wave vector, a-Si supports a vibrational frequency around four times larger than that of a-Se, owing to its higher group velocity. These factors explain the presence of acoustic excitations at frequencies up to 10 THz in a-Si. Other glasses with similar characteristics, such as tetrahedral amorphous carbon, may exhibit such excitations as well, a prediction that can be verified with further inelastic scattering experiments.

V. CONCLUSION

In summary, we report the observation of thermal acoustic excitations with atomic-scale wavelengths in a-Si despite the atomic disorder. The excitations possess wavelengths as small as 6 Å and are supported due to the monatomic composition and high group velocity of a-Si. Our findings demonstrate that the description of thermal vibrations in a-Si as a gas of acoustic excitations is unexpectedly accurate despite the lack of crystalline order, suggesting that other monoatomic glasses with high sound velocity may also support acoustic waves in the thermal spectrum.

ACKNOWLEDGMENTS

The authors thank Nathan Sangkook Lee for helpful discussions in sample preparations, Dr. Jörg Neuefeind and Michelle Everett for assistance in data collection at NOMAD, and Dr. Bianca Haberl for helpful discussions. The authors thank Dr. John Budai for assistance in data collection at HERIX-30. This work was supported by a Samsung Scholarship and a Resnick Fellowship from the Resnick Sustainability Institute at Caltech, and the U.S. Department of Energy, Office of Science, Basic Energy Sciences, Materials Sciences and Engineering Division. This research used resources of the Advanced Photon Source, a U.S. Department of Energy (DOE) Office of Science User Facility operated for the DOE Office of Science by Argonne National Laboratory under Contract No. DE-AC02-06CH11357. A portion of this research used resources at the Spallation Neutron Source, a DOE Office of Science User Facility operated by the Oak Ridge National Laboratory.

This paper has been co-authored by employees of UT-Battelle, LLC, under Contract No. DE AC0500OR22725 with the U.S. Department of Energy. The United States Government retains and the publisher, by accepting the article for publication, acknowledges that the United States Government retains a nonexclusive, paid-up, irrevocable, worldwide license to publish or reproduce the published form of this paper, or allow others to do so, for the United States Government purposes. The Department of Energy will provide public access to these results of federally sponsored research in accordance with the DOE Public Access Plan.

J.M. and A.J.M. conceived the project. J.M. synthesized the a-Si samples. J.M., A.A., A.H.S, R.P.H., and M.E.M conducted the IXS experiments and analyzed the results. R.P.H. performed the RDF measurements. J.M. performed molecular dynamics calculations. J.M. and A.J.M. wrote the paper with input from all authors. A.J.M. supervised the project.

The authors declare no competing interests.

[1] T. S. Grigera, V. Martín-Mayor, G. Parisi, and P. Verrocchio, Phonon interpretation of the 'boson peak' in supercooled liquids, Nature **422**, 289 (2003).

[2] H. Shintani and H. Tanaka, Universal link between the boson peak and transverse phonons in glass, Nat. Mater. **7**, 870 (2008).

[3] V. Lubchenko and P. G. Wolynes, The origin of the boson peak and thermal conductivity plateau in low-temperature glasses, Proc. Natl. Acad. Sci. **100**, 1515 (2003).

[4] B. L. Zink and F. Hellman, Specific heat and thermal conductivity of low-stress amorphous Si-N membranes, Solid State Commun. **129**, 199 (2004).

[5] B. L. Zink, R. Pietri, and F. Hellman, Thermal Conductivity and Specific Heat of Thin-Film Amorphous Silicon, Phys. Rev. Lett. **96**, 055902 (2006).

[6] A. I. Chumakov, G. Monaco, A. Monaco, W. A. Crichton, A. Bosak, R. Rüffer, A. Meyer, F. Kargl, L. Comez, D. Fioretto, H. Giefers, S. Roitsch, G. Wortmann, M. H. Manghnani, A. Hushur, Q. Williams, J. Balogh, K. Parliński, P. Jochym, and P. Piekarz, Equivalence of the Boson Peak in Glasses to the Transverse Acoustic Van Hove Singularity in Crystals, Phys. Rev. Lett. **106**, 225501 (2011).

[7] A. I. Chumakov, G. Monaco, A. Fontana, A. Bosak, R. P. Hermann, D. Bessas, B. Wehinger, W. A. Crichton, M. Krisch, R. Rüffer, G. Baldi, G. Carini Jr., G. Carini, G. D'Angelo, E. Gilioli, G. Tripodo, M. Zanatta, B. Winkler, V. Milman, K. Refson, M. T. Dove, N. Dubrovinskaia, L. Dubrovinsky, R. Keding, and Y. Z. Yue, Role of Disorder in the Thermodynamics and Atomic Dynamics of Glasses, Phys. Rev. Lett. **112**, 025502 (2014).

[8] P. Debye, Zur theorie der spezifischen Wärmen, Ann. Phys. **344**, 789 (1912).

[9] D. A. Parshin, Soft potential model and universal properties of glasses, Phys. Scr. **T49A**, 180 (1993).

[10] D. A. Parshin, H. R. Schober, and V. L. Gurevich, Vibrational instability, two-level systems, and the boson peak in glasses, Phys. Rev. B **76**, 064206 (2007).

[11] F. Léonforte, A. Tanguy, J. P. Wittmer, and J.-L. Barrat, Inhomogeneous Elastic Response of Silica Glass, Phys. Rev. Lett. **97**, 055501 (2006).

[12] B. Dorner and H. Peisl, An instrument with very high energy resolution in X-ray scattering, Nucl. Instrum. Methods Phys. Res. **208**, 587 (1983).

[13] E. Burkel, Phonon spectroscopy by inelastic x-ray scattering, Rep. Prog. Phys. **63**, 171 (2000).

[14] H. Sinn, Spectroscopy with meV energy resolution, J. Phys.: Condens. Matter **13**, 7525 (2001).

[15] M. Krisch and F. Sette, Inelastic x-ray scattering from phonons, in *Light Scattering in Solids IX* (Springer, Berlin, Heidelberg, 2006), pp. 317–370.

[16] A. Q. R. Baron, High-resolution inelastic x-ray scattering I: Context, spectrometers, samples, and superconductors, in *Synchrotron Light Sources and Free-Electron Lasers* (Springer, Cham, 2015), pp. 1–68.

[17] R. Dell'Anna, G. Ruocco, M. Sampoli, and G. Viliani, High Frequency Sound Waves in Vitreous Silica, Phys. Rev. Lett. **80**, 1236 (1998).

[18] D. Fioretto, U. Buchenau, L. Comez, A. Sokolov, C. Masciovecchio, A. Mermet, G. Ruocco, F. Sette, L. Willner, and B. Frick, High-frequency dynamics of glass-forming polybutadiene, Phys. Rev. E **59**, 4470 (1999).

[19] G. Ruocco, F. Sette, R. Di Leonardo, D. Fioretto, Michael Krisch, Maren Lorenzen, Claudio Masciovecchio, G. Monaco, F. Pignon, and T. Scopigno, Nondynamic Origin of the High-Frequency Acoustic Attenuation in Glasses, Phys. Rev. Lett. **83**, 5583 (1999).

[20] T. Scopigno, R. Di Leonardo, G. Ruocco, A. Q. R. Baron, S. Tsutsui, F. Bossard, and S. N. Yannopoulos, High Frequency Dynamics in a Monatomic Glass, Phys. Rev. Lett. **92**, 025503 (2004).

[21] T. Scopigno, J.-B. Suck, R. Angelini, F. Albergamo, and G. Ruocco, High-Frequency Dynamics in Metallic Glasses, Phys. Rev. Lett. **96**, 135501 (2006).

[22] B. Rufflé, G. Guimbretière, E. Courtens, R. Vacher, and G. Monaco, Glass-Specific Behavior in the Damping of Acoustic-like Vibrations, Phys. Rev. Lett. **96**, 045502 (2006).

[23] F. Sette, G. Ruocco, M. Krisch, U. Bergmann, C. Masciovecchio, V. Mazzacurati, G. Signorelli, and R. Verbeni, Collective Dynamics in Water by High Energy Resolution Inelastic X-Ray Scattering, Phys. Rev. Lett. **75**, 850 (1995).

[24] H. Sinn, F. Sette, U. Bergmann, Ch. Halcoussis, M. Krisch, R. Verbeni, and E. Burkel, Coherent Dynamic Structure Factor of Liquid Lithium by Inelastic X-Ray Scattering, Phys. Rev. Lett. **78**, 1715 (1997).

[25] H. Sinn, B. Glorieux, L. Hennet, A. Alatas, M. Hu, E. E. Alp, F. J. Bermejo, D. L. Price, and M.-L. Saboungi, Microscopic dynamics of liquid aluminum oxide, Science **299**, 2047 (2003).

[26] A. Alatas, A. H. Said, H. Sinn, E. E. Alp, C. N. Kodituwakku, B. Reinhart, M. L. Saboungi, and D. L. Price, Elastic modulus of supercooled liquid and hot solid silicon measured by inelastic x-ray scattering, J. Phys. Chem. Solids **66**, 2230 (2005).

[27] P. Benassi, M. Krisch, C. Masciovecchio, V. Mazzacurati, G. Monaco, G. Ruocco, F. Sette, and R. Verbeni, Evidence of High

Frequency Propagating Modes in Vitreous Silica, Phys. Rev. Lett. **77**, 3835 (1996).

[28] G. Monaco and V. M. Giordano, Breakdown of the Debye approximation for the acoustic modes with nanometric wavelengths in glasses, Proc. Natl. Acad. Sci. **106**, 3659 (2009).

[29] L. Orsingher, G. Baldi, A. Fontana, L. E. Bove, T. Unruh, A. Orecchini, C. Petrillo, N. Violini, and F. Sacchetti, High-frequency dynamics of vitreous $GeSe_2$, Phys. Rev. B **82**, 115201 (2010).

[30] E. A. A. Pogna, C. Rodríguez-Tinoco, M. Krisch, J. Rodríguez-Viejo, and T. Scopigno, Acoustic-like dynamics of amorphous drugs in the THz regime, Sci. Rep. **3**, 2518 (2013).

[31] F. H. Stillinger and T. A. Weber, Computer simulation of local order in condensed phases of silicon, Phys. Rev. B **31**, 5262 (1985).

[32] R. L. C. Vink, G. T. Barkema, W. F. van der Weg, and N. Mousseau, Fitting the Stillinger-Weber potential to amorphous silicon, J. Non-Cryst. Solids **282**, 248 (2001).

[33] J. Tersoff, Empirical interatomic potential for silicon with improved elastic properties, Phys. Rev. B **38**, 9902 (1988).

[34] J. Tersoff, Modeling solid-state chemistry: Interatomic potentials for multicomponent systems, Phys. Rev. B **39**, 5566 (1989).

[35] P. B. Allen, J. L. Feldman, J. Fabian, and F. Wooten, Diffusons, locons and propagons: Character of atomic vibrations in amorphous Si, Philos. Mag. B **79**, 1715 (1999).

[36] J. Fabian, J. L. Feldman, C. S. Hellberg, and S. M. Nakhmanson, Numerical study of anharmonic vibrational decay in amorphous and paracrystalline silicon, Phys. Rev. B **67**, 224302 (2003).

[37] Y. He, D. Donadio, and G. Galli, Heat transport in amorphous silicon: Interplay between morphology and disorder, Appl. Phys. Lett. **98**, 144101 (2011).

[38] J. M. Larkin and A. J. H. McGaughey, Thermal conductivity accumulation in amorphous silica and amorphous silicon, Phys. Rev. B **89**, 144303 (2014).

[39] H. R. Seyf and A. Henry, A method for distinguishing between propagons, diffusions, and locons, J. Appl. Phys. **120**, 025101 (2016).

[40] W. Lv and A. Henry, Direct calculation of modal contributions to thermal conductivity via Green-Kubo modal analysis, New J. Phys. **18**, 013028 (2016).

[41] Y. M. Beltukov, C. Fusco, D. A. Parshin, and A. Tanguy, Boson peak and Ioffe-Regel criterion in amorphous siliconlike materials: The effect of bond directionality, Phys. Rev. E **93**, 023006 (2016).

[42] J. Moon, B. Latour, and A. J. Minnich, Propagating elastic vibrations dominate thermal conduction in amorphous silicon, Phys. Rev. B **97**, 024201 (2018).

[43] D. G. Cahill, M. Katiyar, and J. R. Abelson, Thermal conductivity of a-Si: H thin films, Phys. Rev. B **50**, 6077 (1994).

[44] H. Sinn, E. E. Alp, A. Alatas, J. Barraza, G. Bortel, E. Burkel, D. Shu, W. Sturhahn, J. P. Sutter, and T. S. Toellner, An inelastic x-ray spectrometer with 2.2 meV energy resolution, Nucl. Instrum. Methods Phys. Res., Sect. A **467–468**, 1545 (2001).

[45] A. Alatas, B. M. Leu, J. Zhao, H. Yavaş, T. S. Toellner, and E. E. Alp, Improved focusing capability for inelastic x-ray spectrometer at 3-ID of the APS: A combination of toroidal and Kirkpatrick-Baez (KB) mirrors, Nucl. Instrum. Methods Phys. Res., Sect. A **649**, 166 (2011).

[46] A. H. Said, H. Sinn, and R. Divan, New developments in fabrication of high-energy-resolution analyzers for inelastic x-ray spectroscopy, J. Synchrotron Radiat. **18**, 492 (2011).

[47] T. S. Toellner, A. Alatas, and A. H. Said, Six-reflection meV-monochromator for synchrotron radiation, J. Synchrotron Radiat. **18**, 605 (2011).

[48] F. de Brito Mota, J. F. Justo, and A. Fazzio, Structural properties of amorphous silicon nitride, Phys. Rev. B **58**, 8323 (1998).

[49] X. Liu, J. L. Feldman, D. G. Cahill, R. S. Crandall, N. Bernstein, D. M. Photiadis, M. J. Mehl, and D. A. Papaconstantopoulos, High Thermal Conductivity of a Hydrogenated Amorphous Silicon Film, Phys. Rev. Lett. **102**, 035901 (2009).

[50] See Supplemental Material at http://link.aps.org/supplemental/10.1103/PhysRevMaterials.3.065601 for the inelastic peak broadening comparison between current work and prior predictions.

[51] P. B. Allen and J. L. Feldman, Thermal conductivity of disordered harmonic solids, Phys. Rev. B **48**, 12581 (1993).

[52] F. Sette, M. H. Krisch, C. Masciovecchio, G. Ruocco, and G. Monaco, Dynamics of glasses and glass-forming liquids studied by inelastic x-ray scattering, Science **280**, 1550 (1998).

[53] P. M. Voyles, N. Zotov, S. M. Nakhmanson, D. A. Drabold, J. M. Gibson, M. M. J. Treacy, and P. Keblinski, Structure and physical properties of paracrystalline atomistic models of amorphous silicon, J. Appl. Phys. **90**, 4437 (2001).

[54] M. M. J. Treacy and K. B. Borisenko, The local structure of amorphous silicon, Science **335**, 950 (2012).

[55] G. T. Barkema and N. Mousseau, High-quality continuous random networks, Phys. Rev. B **62**, 4985 (2000).

[56] S. N. Taraskin and S. R. Elliott, Low-frequency vibrational excitations in vitreous silica: The Ioffe-Regel limit, J. Phys.: Condens. Matter **11**, A219 (1999).

[57] S. Munetoh, T. Motooka, K. Moriguchi, and A. Shintani, Interatomic potential for Si-O systems using Tersoff parametrization, Comput. Mater. Sci. **39**, 334 (2007).

[58] B. Cros, E. Gat, and J. M. Saurel, Characterization of the elastic properties of amorphous silicon carbide thin films by acoustic microscopy, J. Non-Cryst. Solids **209**, 273 (1997).

[59] M. Foret, B. Hehlen, G. Taillades, E. Courtens, R. Vacher, H. Casalta, and B. Dorner, Neutron Brillouin and Umklapp Scattering from Glassy Selenium, Phys. Rev. Lett. **81**, 2100 (1998).